Study of phonon modes in silicon nanocrystals using the adiabatic bond charge model

2008 J. Phys.: Condens. Matter 20 145213

(http://iopscience.iop.org/0953-8984/20/14/145213)

IOP PUBLISHING JOURNAL OF PHYSICS: CONDENSED MATTER

J. Phys.: Condens. Matter **20** (2008) 145213 (8pp) doi:10.1088/0953-8984/20/14/145213

Study of phonon modes in silicon nanocrystals using the adiabatic bond charge model

Audrey Valentin, Johann Sée, Sylvie Galdin-Retailleau and Philippe Dollfus

Institut d'Electronique Fondamentale, Université Paris-Sud, CNRS, 91405 Orsay, France

E-mail: audrey.valentin@ief.u-psud.fr

Received 23 January 2008, in final form 29 February 2008
Published 19 March 2008
Online at stacks.iop.org/JPhysCM/20/145213

Abstract

We present theoretical calculations of phonon dispersion in silicon nanocrystals using an approach based on the adiabatic bond charge model. To deal with the boundary conditions, two cases are considered: the surface atoms are either free to move or rigidly fixed. In the former case, surface modes appear at low frequencies and, in the latter case, nodes and antinodes appear near a frequency of 11 THz. By projecting the nanocrystal modes on the basis of bulk modes, one can show the increasing correlation between the nanocrystal modes and the bulk modes when increasing the dot size. Finally, the frequency shift of Raman spectra calculated as a function of the dot size is found to be in good agreement with sets of experimental data.

(Some figures in this article are in colour only in the electronic version)

1. Introduction

Due to their compatibility with CMOS (complementary metal–oxide–semiconductor) technology, silicon nanocrystals are likely to become a key element of integrated nanodevices as single-electron transistors [7] or flash memories [11, 41]. With this aim in mind, to fully assess the potentialities of electronic devices based on semiconductor quantum dots it is important to understand precisely the mechanisms of electron–phonon interaction in semiconductor nanocrystals and their consequences for the electron dynamics. According to several authors [1, 2, 25, 45], the discrete nature of electron levels in quantum dots is expected to give rise to the phenomenon called phonon bottleneck: an electron on an excited level cannot relax to the fundamental one by inelastic phonon scattering unless the energy level separation is exactly equal to the phonon energy, which is likely to yield slow relaxation effects. However, more detailed analyses have predicted that the phonon bottleneck should weaken or even disappear because of multiphonon effects [22] and collisional broadening [23, 24]. Studies of the consequences of collisional broadening for electron relaxation in semiconductor quantum dots have been reported for GaAs quantum dots using bulk phonon energies [29, 39]. Nevertheless, as for electrons, the strong confinement in nanocrystals modifies the phonon states and consideration of the correct phonon dispersion is certainly important to accurately describe the electron–phonon coupling.

In section 2, we present the main features of the simulation method based on Weber's adiabatic bond charge model (ABCM) [47], first applied here to bulk silicon and then to silicon nanocrystals by introducing an effective Madelung constant. In section 3, the results obtained for silicon nanocrystals are reported and discussed as a function of nanocrystal radius by comparison with bulk properties. A comparison with experimental data is also presented.

2. The model

In the harmonic approximation the displacements $\vec{u}$ are assumed to be small compared to the interatomic distance. The motion equation is thus written as [3, 4, 9, 10, 31, 38]

$$M\omega^2\vec{u} = D\vec{u} \tag{1}$$

where M is the mass of the silicon atom, ω the vibrational frequency and D the dynamical matrix.

The problem is now to build the dynamical matrix, that is to establish an appropriate expression for the force constant

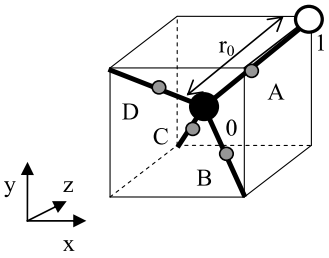

Figure 1. Unit cell in the BCM and the ABCM.

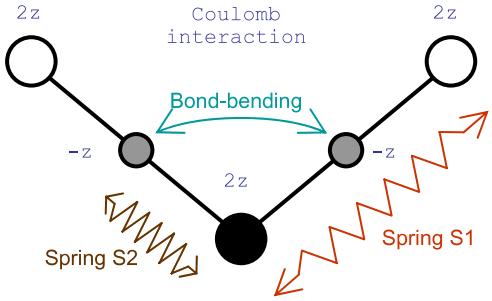

Figure 2. Interactions of the ABCM.

elements. Since it expresses the interactions between the atoms of the crystal, this expression should depend on the model used. We have chosen to use Weber's adiabatic bond charge model (ABCM) [47] which has been shown to give very good results for bulk diamond and zinc-blende-type crystals [48]. Due to its efficiency, the ABCM has been successfully used to calculate the phonon dispersion for III–V crystals [37], for II–VI materials [35], as well as nitride compounds GaN, AlN, BN [44], for GaAs [42] and InP [43] surfaces and more recently for various silicon nanostructures including rectangular silicon nanowires [18] and lattices of nanocrystals [19, 20].

Earlier models, such as Cochran's shell model [4, 8–10, 38], have already provided good agreement with experiment. Based on an idea of Dick and Overhauser [12], the shell model proposes to split the atoms in two parts: a shell of valence electrons surrounding a core, assimilated to a positive ion. Phillips [34] pointed out the lack of physical meaning of the shell model: due to the nature of the covalent bond, electrons should be shared between the two neighbouring atoms. He proposed to model the shared electrons by a negative point charge located on the bonds: the bond charges. This idea was used later by Martin when creating the bond charge model (BCM) [32], where the bond charges are rigidly located midway from the neighbouring ions; the unit cell for bulk diamond-type semiconductors contains two ions, denoted 0 and 1, and four bond charges, denoted here by A, B, C and D (as indicated in figure 1). The dispersion relation for silicon was well reproduced, except for the transverse acoustic (TA) branch flattening at high wavevector. Weber later explained this flattening by the motion of bond charges [46] and extended the BCM to the ABCM where the bond charges are allowed to move.

To complete the ABCM, the number and type of interactions have to be properly chosen. Weber introduced four types of interactions, which are schematized in figure 2.

- A central force S1, which can be represented by a spring between the two ion cores of the unit cell. This central force is identical to the one used in the force constant model [3, 4, 9, 10, 31, 38].
- A Keating-type bond-bending interaction, inspired by Keating's model [26], between the bond charges.
- Since the total charge of an atom is now separated between a bond charge and the ion core, we need to use a set of Coulomb interactions similar to the one used in the BCM, which relies on the rigid-ion model [3, 4, 9, 10, 27, 31, 38]. The intensity of the Coulomb interactions depends on the magnitude of the charge borne by the bond charges z. Due to electrical neutrality of the unit cell, the ions which are linked to four ions bear the charge $-2z$.

A new problem arises: the number of degrees of freedom of the problem is too high, and we now have to deal with several dynamical matrices. As in the shell model, Weber used the adiabatic approximation which assumes that the bond charges have a zero mass and that they follow the ionic motion adiabatically.

Lastly, to guarantee the equilibrium of the system, the total energy per atom has to be minimized (this is the equilibrium condition). We then have to solve the equation given in the appendix of [47], which involves the Madelung constant α_M [28]. This constant will be discussed further in the next subsections.

2.1. Application of the model to bulk silicon

We first apply the ABCM to bulk silicon with the same parameters as those used by Weber [47].

As illustrated in figure 1, the unit cell contains two ions and four bond charges. Given that the real space is three dimensional, the dimension of the dynamical matrix is 6×6. The determination of the eigenvalues and eigenvectors is thus easy, although the operation must be performed for each wavevector.

The crystal being infinite and the Coulomb interaction being long-range, the Coulombic part of the dynamical matrix is a sum over an infinite distribution of point charges. Such calculations take long to converge; conveniently, the Ewald transformation [3, 4, 31], which consists in introducing Gaussian charge distributions, may be used to get much faster convergence.

The Madelung constant α_M is defined by:

$$\alpha_M = -\frac{r_0}{4}\frac{1}{2}\sum_{i,j}^{\infty}\frac{\varsigma_i\varsigma_j}{R^j - R^i} \tag{2}$$

where r_0 is the equilibrium bond length. If z is the minimal charge in the lattice (here it is the charge of the bond charge) and if z_i is the charge of the ion or bond charge i, we have $z_i = \zeta_i z$. We use the value of 4.453 evaluated by Martin for bulk silicon [32].

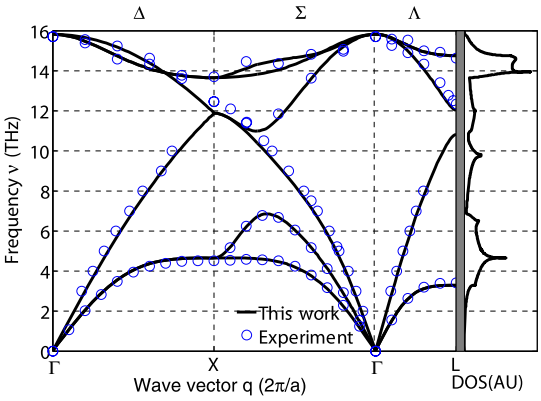

Figure 3. Calculated phonon dispersion relation for bulk silicon compared to experiment and its calculated density of states (arbitrary units).

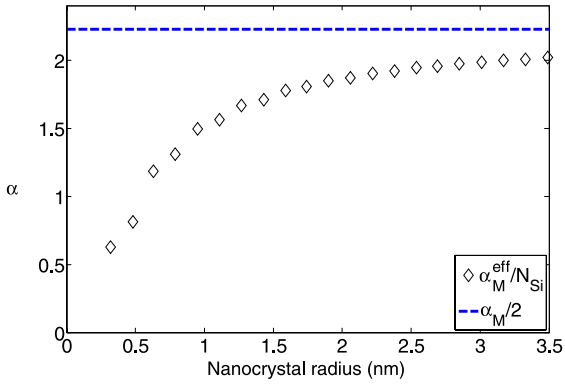

Figure 4. Effective Madelung constant per atom α_M^{eff}/N_{Si} in nanocrystals compared to the actual Madelung constant per atom $\alpha_M/2$ in bulk material.

The calculated phonon dispersion for bulk silicon compared to experimental data [30] is plotted in figure 3. The agreement is good and even the TA flattening is properly reproduced. Figure 3 also shows the calculated density of states (DOS) which exhibits two main peaks, one near 5 THz and the other at 14–15 THz. The first peak corresponds to the flattening of the TA branch at the Brillouin zone edge and the second one to the optical branches.

2.2. Application of the model to silicon nanocrystals

Owing to the breaking of the translational symmetry, the notions of wavevector and unit cell are meaningless. The whole nanocrystal has to be taken into account.

For an N_{Si}-atom nanocrystal, we first determine the number N_{BC} of bond charges (which is the same as the number of bounds in the nanocrystal). The dimensions of the dynamical matrix D are now $3N_{Si} \times 3N_{Si}$. The determination of its eigenvalues and eigenvectors can thus be computationally demanding. Moreover, with a finite nanocrystal, the Ewald transformation cannot be applied anymore but finite summations have to be computed.

The equilibrium condition requires the rewriting of the effective Madelung constant, defined as

$$\alpha_M^{eff} = -\frac{r_0}{4}\frac{1}{2}\sum_{i,j}^{N_{Si}+N_{BC}} \frac{\varsigma_i \varsigma_j}{R^j - R^i}. \tag{3}$$

As shown in figure 4, α_M^{eff}/N_{Si} tends slowly to $\alpha_M/2$ as the nanocrystal radius tends to infinity. Except for the change in this constant, we keep the same parameters for nanocrystals as those used for bulk silicon.

We now have to deal with the problem of boundary conditions, since in practical applications the silicon nanocrystal should be embedded in silicon dioxide. As the specific vibrational properties of the atoms situated at the oxide interface are unknown, two extreme cases are treated: the atoms are considered either fully free to move (free boundary conditions) or are kept motionless (clamped boundary conditions). The detailed analysis of the Si/SiO_2 interface is beyond the scope of this paper and other cases of boundary conditions are not considered here. These two types of boundary conditions have already been discussed for nanowires [40] and layers [13].

3. Results

The frequency and amplitude of vibrations have been calculated for silicon nanocrystals of various sizes.

For each nanocrystal, we determine the phonon density of states (DOS) and compare it to the bulk DOS. When the nanocrystal radius increases, the two DOS must get closer and closer [16, 19, 20]. The comparison is possible as the areas under the curves are normalized to 1.

To complete the analysis, a projection method is applied to compare the nanocrystal modes with bulk modes. The continuous ensemble of bulk eigenvectors is restricted to obtain a discrete basis of vectors with the same number of elements as the nanocrystal eigenvector. The Born–von Karman cyclic boundary conditions are used to limit the number of wavevectors and then the bulk vectors $\vec{u}_B(\vec{q}, \omega_B)$ form a basis set on which the nanocrystal modes $\vec{u}_{NC}(\omega_{NC})$ are projected

$$\vec{u}_{NC}(\omega_{NC}) = \sum_{\vec{q},\omega_B} C(\vec{q}, \omega_B, \omega_{NC}) \cdot \vec{u}_B(\vec{q}, \omega_B). \tag{4}$$

If the nanocrystal modes are strongly correlated to the bulk modes, the projection coefficient $C(\vec{q}, \omega_B, \omega_{NC})$ must be high and localized around a given frequency [16, 21]. As an example, a nanocrystal phonon of high frequency is expected to be related to a bulk optic phonon, which should lead to a high projection coefficient C. Due to the great number of projection coefficients, we define some quantities to make the analysis easier. First, we use the total coherence term defined by

$$B(\vec{q}, \omega_{NC}) = \sum_{\omega_B} C(\vec{q}, \omega_B, \omega_{NC}) \tag{5}$$

which expresses the global correlation between a nanocrystal mode and the bulk modes with wavevector $\vec{q}$.

This quantity can be represented as a surface superimposed on the bulk dispersion relation. If the correlation is good, we should obtain a high total coherence term for $\omega_{NC} \approx \omega_B(\vec{q})$

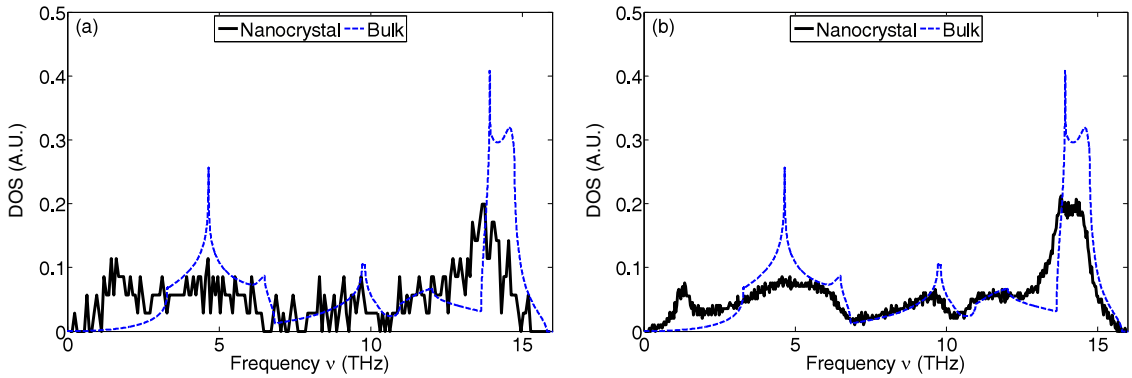

Figure 5. DOS calculated considering free boundary conditions for nanocrystals of radius: (a) 0.6 nm; (b) 2.5 nm; the bulk DOS is represented by dashed lines.

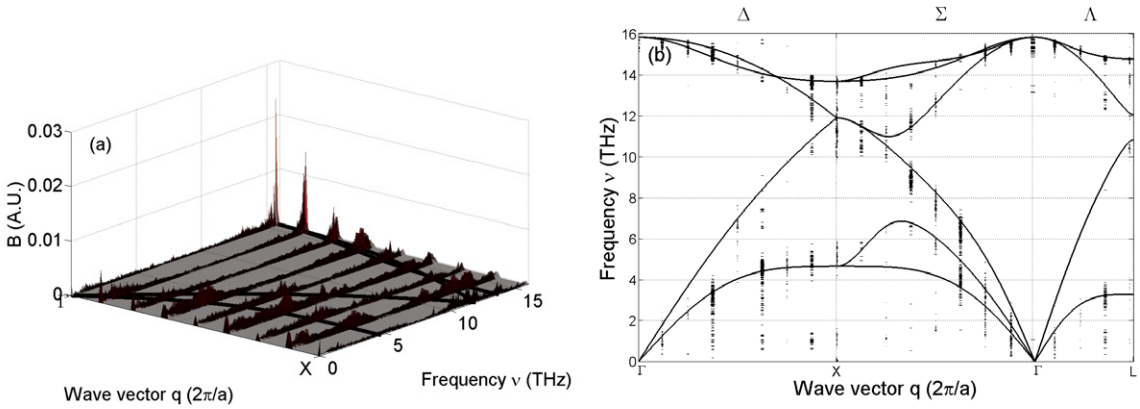

Figure 6. Total coherence term considering free boundary conditions for a 2.5 nm-radius nanocrystal (lines, bulk dispersion relation): (a) 3D plot in the [1, 0, 0] direction; (b) contour plot.

and the surface should exhibit a peak. Then, to determine where the nanocrystal modes are located in the bulk Brillouin zone, we calculate the Brillouin zone localization as

$$L(\vec{q}) = \sum_{\omega_B, \omega_{NC}} C(\vec{q}, \omega_B, \omega_{NC}). \quad (6)$$

3.1. Free-standing boundary conditions

In case of free surface atoms, it can be seen from figure 5 that the global shape of the nanocrystal DOS tends to the bulk DOS. However, for two frequency ranges (from 0 to 2 THz and from 13 to 14 THz) the dot modes do not correspond to bulk modes. In figure 6 the total coherence term $B(\vec{q}, \omega_{NC})$ is represented for wavevectors in the direction [1, 0, 0]. The coherence seems good, except for the same frequency range where the peaks are delocalized over the whole range of wavevectors: these modes are correlated to all the bulk modes at the same time. They are specific modes of the nanocrystal.

We shall now have a look at the Brillouin zone localization (figure 7). It appears clearly that the nanocrystal modes are mostly correlated to the bulk zone centre modes. Thus, the modes related to the zone edge modes, as the TA modes, are not visible in the nanocrystal. This explains why the TA peak at 4–5 THz is not reproduced in figure 5.

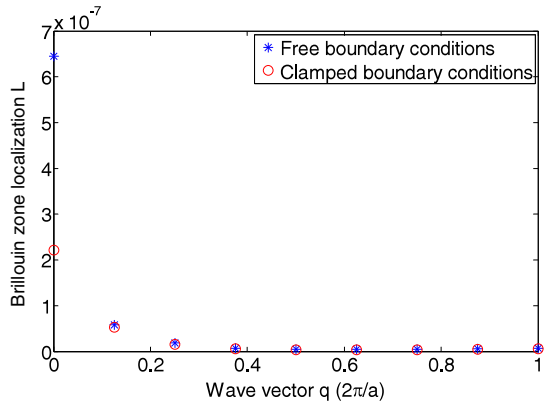

Figure 7. Brillouin zone localization for a 2.5 nm-radius nanocrystal.

After explaining the appearance of some specific modes, we can consider these results as a first indication that the model is correct.

While studying GaP nanocrystals, Fu *et al* [16] demonstrated the existence of surface-like modes. Such modes have also been observed by Tütüncü and Srivastava for GaAs [42] and InP surfaces [43]. As shown in figure 8 for one of the specific modes ($\nu = 2$ THz), the vibration amplitude

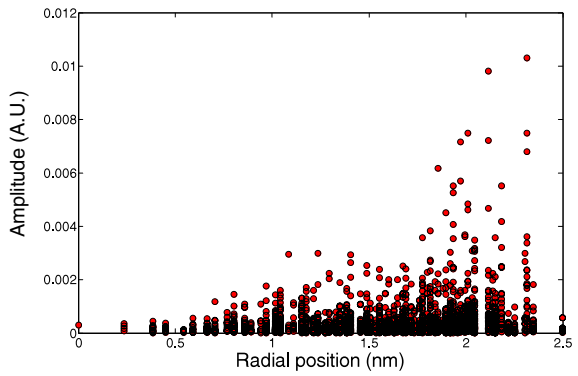

Figure 8. Amplitude of vibration of atoms in a nanocrystal ($R = 2.5$ nm) as a function of their radial position considering free boundary conditions. The mode frequency is $\nu = 2$ THz.

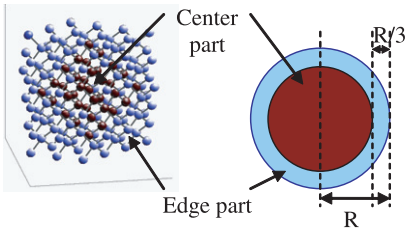

Figure 9. Separation of the nanocrystal between a centre part and an edge part.

is maximal near the surface of the nanocrystal: surface-like modes actually appear. We thus divide the 2.5 nm nanocrystal DOS into two parts (figure 9): one considering only the atoms in the centre, the other considering the atoms at the edge of the nanocrystal. The boundary is arbitrarily set at a radius of two-thirds of the total radius of the nanocrystal.

It appears clearly in figure 10 that the centre DOS (a) is very close to the bulk DOS whereas the edge DOS (b) displays mostly the specific modes. We thus conclude that these specific ranges constitute surface-like modes while the others are bulk-like modes.

It should be emphasized that, dealing with free boundary conditions, the relaxation of the surface atoms has not been taken into account. Tütüncü and Srivastava demonstrated that some frequencies are slightly shifted and some others appear [42, 43]. We have chosen to neglect this effect, as has been done by other authors [16, 49], considering that the effect of relaxation is negligible. We notice that, due to negative eigenvalues of the dynamical matrix, a few imaginary frequencies of weak magnitude ($\nu < 2$ THz) appear in the results. Fu *et al* also obtained imaginary frequencies in the same approximation [16].

3.2. Clamped boundary conditions

With clamped boundary conditions, the atoms at the Si/SiO_2 interface are fixed to their equilibrium positions. This is achieved by setting to zero appropriate elements of the dynamical matrix. Relaxation of the surface atoms is then meaningless and in this case there are no imaginary frequencies.

It must be noted from figure 11 that the global shape of the nanocrystal DOS is close to the bulk DOS, except in the 10–11 THz frequency range where an additional peak is observed. The projection of the nanocrystal modes in figure 12 confirms the existence of this specific frequency range.

Again, the Brillouin zone localization in the [1, 0, 0] direction (figure 7) shows that the nanocrystal modes are mostly related to bulk zone centre modes.

Then, forgetting the specific modes, we can still consider this result as a good indication that the model is correct. For these modes, it appears that the vibration amplitude exhibits a succession of nodes and antinodes as a function of their radial position (figure 13).

The specific modes in silicon nanocrystal pointed out in this paper, using the two types of boundary conditions, did not appear in earlier calculations, probably due to the use of supercell geometry [19, 20] and periodic boundary conditions [21].

3.3. Comparison with experiments

Raman spectra have been measured for nanocrystals of various sizes [14, 17]. It appears that for nanocrystals of radius greater than 10 nm the bulk spectrum is recovered, while for small nanocrystals we have two peaks, one at high frequency

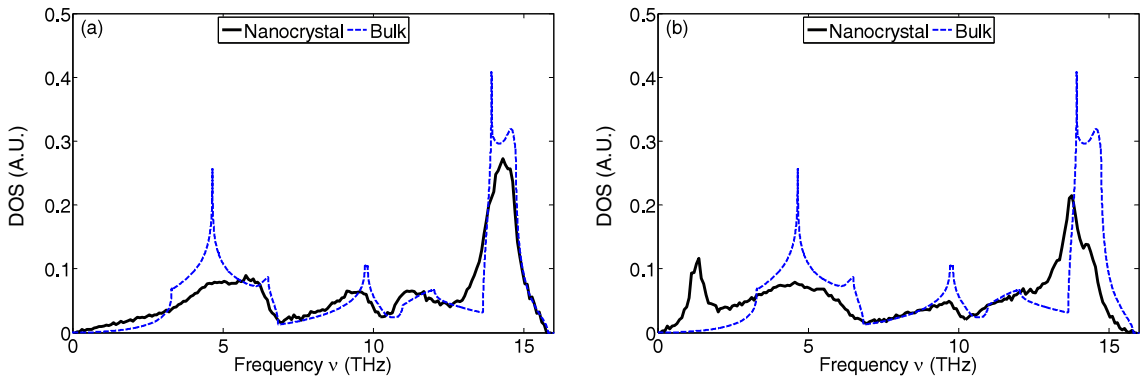

Figure 10. (a) DOS calculated for the atoms at the centre of the nanocrystal. (b) DOS calculated for the atoms at the edge of the nanocrystal. The radius is 2.5 nm; bulk DOS is represented in dashed lines, free boundary conditions are considered.

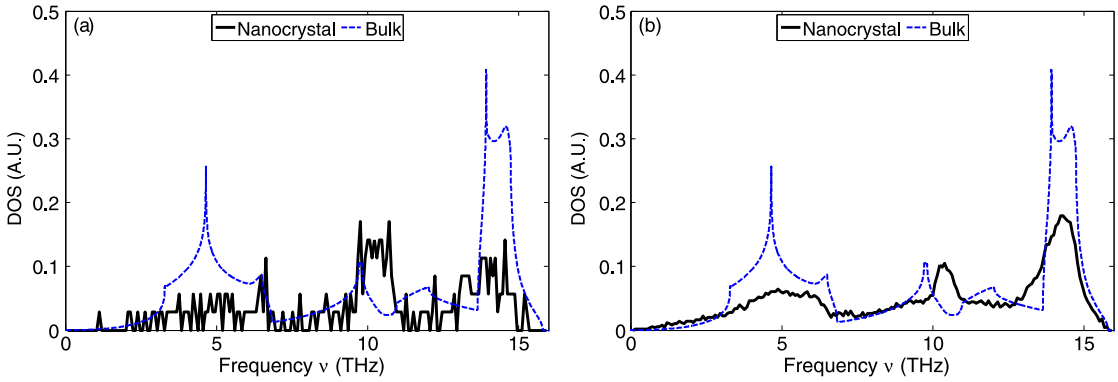

Figure 11. DOS calculated by considering clamped boundary conditions for nanocrystals of radius: (a) 0.6 nm; (b) 2.5 nm; the bulk DOS is represented by dashed lines.

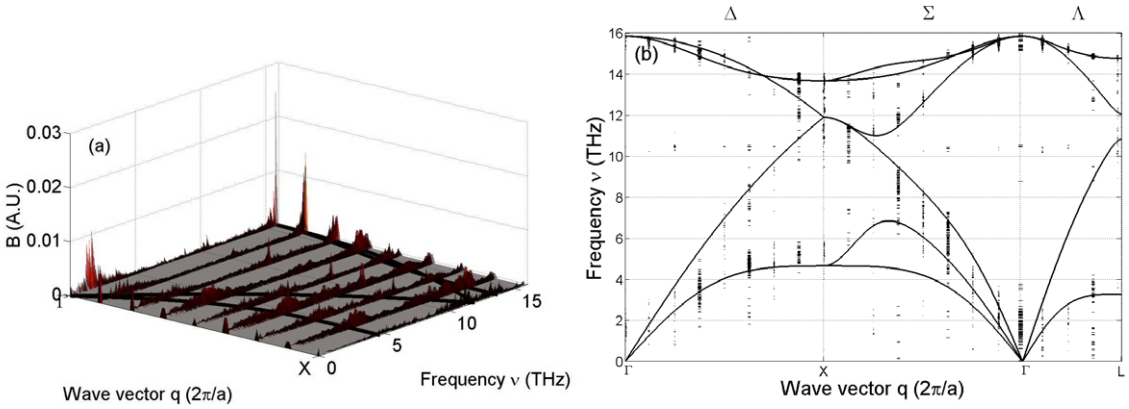

Figure 12. Total coherence term considering clamped boundary conditions for a 2.5 nm-radius nanocrystal (lines, bulk dispersion relation): (a) 3D plot in the [1, 0, 0] direction; (b) contour plot.

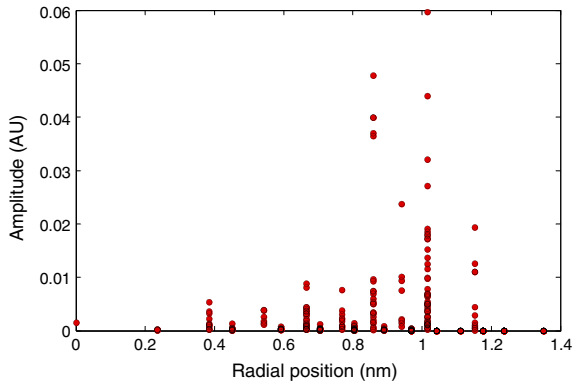

Figure 13. Amplitude of vibration of atoms of a nanocrystal ($R = 1.35$ nm) as a function of their radial position considering clamped boundary conditions (the mode frequency is $\nu = 10.5$ THz).

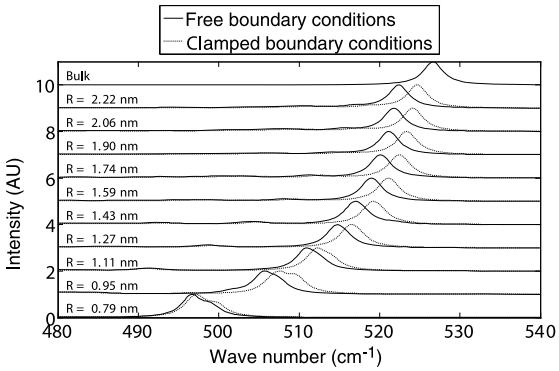

Figure 14. Calculated Raman spectra for nanocrystals of various sizes and for bulk silicon.

approaching the main bulk peak [14], the other at very low frequency tending to zero [17] with increasing dot size.

Raman spectra can also be calculated from the phonon wavevectors and phonon frequencies. We have adapted Richter's theory [5, 6, 15, 33, 36, 50] and used our projection coefficient $C(\vec{q}, \omega_B, \omega_{NC})$ to reconstruct a Raman spectrum in the form

$$I(\omega) \propto \sum_{\omega_B, \omega_{NC}} \frac{|C(\vec{0}, \omega_B, \omega_{NC})|^2}{[\omega - \omega_{NC}]^2 - (\Gamma_0/2)^2}$$

where Γ_0 is the natural line shape (taken as $\Gamma_0 = 3\ \mathrm{cm}^{-1}$ [15]).

The spectra obtained for nanocrystals of various sizes at high frequencies are displayed in figure 14. The shift of the main peak is clearly shown. This frequency shift is compared

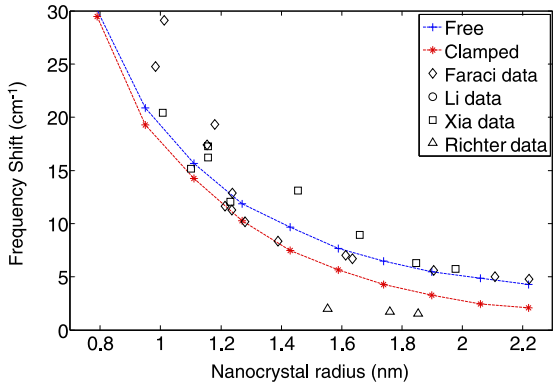

Figure 15. Calculated (broken lines) and experimental Raman shifts at high frequencies.

to experimental data in figure 15. A good agreement is found, which completes the validation of our model. Both boundary conditions give results within the range of experimental results, the spread of which is larger than the difference between the two curves.

4. Conclusion

Using the adiabatic bond charge model and introducing an effective Madelung constant, we have calculated the phonon dispersion of silicon nanocrystals. The boundary conditions are chosen to be either free or clamped.

In the case of free-standing boundary conditions the results are coherent with the bulk case, except for a frequency range which has been demonstrated to correspond to surface vibrations. In the case of clamped boundary conditions the DOS is still close to the bulk one but another specific low frequency range appears with mode amplitudes characterized by nodes and antinodes as a function of the radial distance. Comparison with experimental Raman spectra gives very good results.

These results open up the possibility of an accurate study of electron–phonon coupling and the computation of scattering rates in nanocrystals.

Acknowledgments

This work was partially supported by the European Commission in the frame of the NANOSIL network of Excellence (ICT-216171). The authors acknowledge Mr Damien Querlioz and Pr Arnaud Bournel for fruitful discussions.

References

[1] Benisty H 1995 Reduced electron–phonon relaxation rates in quantum-box systems: theoretical analysis *Phys. Rev.* B **51** 13281–93
[2] Bockelmann U and Bastard G 1990 Phonon scattering and energy relaxation in two-, one-, and zero-dimensional electron gases *Phys. Rev.* B **42** 8947–51
[3] Born M and Huang K 1998 *Dynamical Theory of Crystal Lattices* (Oxford: Oxford University Press)
[4] Brüech P 1982 *Phonons: Theory and Experiments I* (Berlin: Springer)
[5] Campbell I H and Fauchet P M 1986 The effects of microcrystal size and shape on the one phonon Raman spectra of crystalline semiconductors *Solid State Commun.* **58** 739–41
[6] Cheng W and Ren S F 2002 Calculations on the size effects of Raman intensities of silicon quantum dots *Phys. Rev.* B **65** 205305
[7] Choi B H 1998 Fabrication and room-temperature characterization of a silicon self-assembled quantum-dot transistor *Appl. Phys. Lett.* **73** 3129
[8] Cochran W 1959 Theory of the lattice vibrations of germanium *Proc. R. Soc.* A **253** 260–76
[9] Cochran W 1963 Lattice vibrations *Rep. Prog. Phys.* **26** 1–45
[10] Cochran W 1971 Lattice dynamics of ionic and covalent crystals *CRC Crit. Rev. Solid State Sci.* **2** 1–44
[11] De Salvo B, Gerardi C, Lombardo S, Baron T, Perniola L, Mariolle D, Mur P, Toffoli A, Gely M and Semeria M N 2003 How far will silicon nanocrystals push the scaling limits of NVMs technologies? *IEDM'03: Electron Devices Mtg, 2003, Technical Digest* (Piscataway, NJ: IEEE) p 26.1
[12] Dick B G and Overhauser A W 1958 Theory of the dielectric constants of alkali halide crystals *Phys. Rev.* **112** 90–103
[13] Donetti L, Gámiz F, Rodriguez N, Jimenez F and Sampedro C 2006 Influence of acoustic phonon confinement on electron mobility in ultrathin silicon on insulator layers *Appl. Phys. Lett.* **88** 122108
[14] Faraci G, Gibilisco S, Russo P, Pennisi A R, Compagnini G, Battiato S, Puglisi R and La Rosa S 2005 Si/SiO_2 core–shell clusters probed by Raman spectroscopy *Eur. Phys. J.* B **46** 457–61
[15] Faraci G, Gibilisco S, Russo P, Pennisi A R and La Rosa S 2006 Modified Raman confinement model for Si nanocrystals *Phys. Rev.* B **73** 33307
[16] Fu H, Ozolinš V and Zunger A 1999 Phonons in GaP quantum dots *Phys. Rev.* B **59** 2881–7
[17] Fujii M, Kanzawa Y, Hayashi S and Yamamoto K 1996 Raman scattering from acoustic phonons confined in Si nanocrystals *Phys. Rev.* B **54** 8373–6
[18] Hepplestone S P and Srivastava G P 2004 The lattice dynamics of rectangular silicon nanowires *Phys. Status Solidi* c **1** 2617–20
[19] Hepplestone S P and Srivastava G P 2005 Lattice dynamics of ultrasmall silicon nanostructures *Appl. Phys. Lett.* **87** 231906
[20] Hepplestone S P and Srivastava G P 2006 Lattice dynamics of silicon nanostructures *Nanotechnology* **17** 3288–98
[21] Hu X and Zi J 2002 Reconstruction of phonon dispersion in Si nanocrystals *J. Phys.: Condens. Matter* **14** L671–7
[22] Inoshita T and Sakaki H 1992 Electron relaxation in a quantum dot: significance of multiphonon processes *Phys. Rev.* B **46** 7260–3
[23] Inoshita T and Sakaki H 1996 Electron–phonon interaction and the so-called phonon bottleneck effect in semiconductor quantum dots *Physica* B **227** 373–7
[24] Inoshita T and Sakaki H 1997 Density of states and phonon-induced relaxation of electrons in semiconductor quantum dots *Phys. Rev.* B **56** 4355–8
[25] Jiang H and Singh J 1998 Radiative and non-radiative inter-subband transition in self assembled quantum dots *Physica* E **2** 720–4
[26] Keating P N 1966 Effect of invariance requirements on the elastic strain energy of crystals with application to the diamond structure *Phys. Rev.* **145** 637–45
[27] Kellermann E W 1940 Theory of the vibrations of the sodium chloride lattice *Phil. Trans. R. Soc.* A **238** 513–48
[28] Kittel C 1986 *Introduction to Solid State Physics* (New York: Wiley)
[29] Král K and Khás Z 1998 Electron self-energy in quantum dots *Phys. Rev.* B **57** 2061–4

[30] Kulda J, Strauch D, Pavone P and Ishii Y 1994 Inelastic-neutron-scattering study of phonon eigenvectors and frequencies in Si *Phys. Rev.* B **50** 13347–54
[31] Maradudin A A, Montroll E W, Weiss G H and Ipatova I P 1971 *Theory of Lattice Dynamics in the Harmonic Approximation* vol suppl. 3 (New York: Academic)
[32] Martin R M 1969 Dielectric screening model for lattice vibrations of diamond-structure crystals *Phys. Rev.* **186** 871–84
[33] Paillard V, Puech P, Laguna M A, Carles R, Kohn B and Huisken F 1999 Improved one-phonon confinement model for an accurate size determination of silicon nanocrystals *J. Appl. Phys.* **86** 1921
[34] Phillips J C 1968 Covalent bond in crystals I. Elements of a structural theory *Phys. Rev.* **166** 832–8
[35] Rajput B D and Browne D A 1996 Lattice dynamics of II–VI materials using the adiabatic bond-charge model *Phys. Rev.* B **53** 9052–8
[36] Richter H, Wang Z P and Ley L 1981 The one phonon Raman spectrum in microcrystalline silicon *Solid State Commun.* **39** 625–9
[37] Rustagi K C and Weber W 1976 Adiabatic bond charge model for the phonons in A_3B_5 semiconductors *Solid State Commun.* **18** 673–5
[38] Sham L J 1974 *Dynamical Properties of Solids* (Amsterdam: North-Holland)
[39] Stauber T, Zimmermann R and Castella H 2000 Electron–phonon interaction in quantum dots: a solvable model *Phys. Rev.* B **62** 7336–43
[40] Thonhauser T and Mahan G D 2004 Phonon modes in Si[111] nanowires *Phys. Rev.* B **69** 75213
[41] Tiwari S, Farhan R, Hussein H, Allan H, Emmanuel F C and Kevin C 1996 A silicon nanocrystals based memory *Appl. Phys. Lett.* **68** 1377–9
[42] Tütüncü H M and Srivastava G P 1996 Phonon dispersion on a GaAs(110) surface studied using the adiabatic bond charge model *J. Phys.: Condens. Matter* **8** 1345–58
[43] Tütüncü H M and Srivastava G P 1996 Surface phonons on InP(110) with the adiabatic bond-charge model *Phys. Rev.* B **53** 15675–81
[44] Tütüncü H M and Srivastava G P 2000 Phonons in zinc-blende and wurtzite phases of GaN, AlN, and BN with the adiabatic bond-charge model *Phys. Rev.* B **62** 5028–35
[45] Urayama J, Norris T B, Singh J and Bhattacharya P 2001 Observation of phonon bottleneck in quantum dot electronic relaxation *Phys. Rev. Lett.* **86** 4930
[46] Weber W 1974 New bond-charge model for the lattice dynamics of diamond-type semiconductors *Phys. Rev. Lett.* **33** 371–4
[47] Weber W 1977 Adiabatic bond charge model for the phonons in diamond, Si, Ge, and α-Sn *Phys. Rev.* B **15** 4789–803
[48] Yu P Y and Cardona M 2005 *Fundamentals of Semiconductors: Physics and Materials Properties* (Berlin: Springer)
[49] Zi J 1996 Raman shifts in Si nanocrystals *Appl. Phys. Lett.* **69** 200
[50] Zi J, Zhang K and Xie X 1997 Comparison of models for Raman spectra of Si nanocrystals *Phys. Rev.* B **55** 9263–6